Isı Bilimi ve Tekniği Dergisi, 37, 1, 159-170, 2017
J. of Thermal Science and Technology

ISSN 1300-3615

THE EFFECT OF MANUFACTURING LIMITATIONS ON GROOVE DESIGN AND ITS IMPLEMENTATION TO AN ALGORITHM FOR DETERMINING HEAT TRANSPORT CAPABILITY OF HEAT PIPES

Cem ÖMÜR*, Ahmet Bilge UYGUR and İlhami HORUZ*****
*,** Turkish Aerospace Industries, Inc., Fethiye Mah. Havacılık Blv. No:17 06980, Ankara
comur@tai.com.tr, auygur@tai.com.tr
*** Gazi Üniversitesi Müh. Fak., Makine Müh. Böl., Maltepe, Ankara
06570, ilhamihoruz@gazi.edu.tr

(Geliş Tarihi: 27.06.2016, Kabul Tarihi: 14.12.2016)

Abstract: In this study, a methodology for the computation of maximum heat transport capability of grooved heat pipes is presented. The methodology takes into account extrusion limitations together with the vapor, liquid pressure losses along the heat pipe, the temperature drop between evaporator and condenser. The implementation of the methodology to an algorithm and its predictive performance was demonstrated on rectangular, trapezoidal, triangular and re-entrant grooved heat pipes for a specific allowable space and working temperature. It was seen that the heat pipe with re-entrant groove is superior to other geometries in terms of heat transport capacity.
Keywords: Grooved heat Pipe, Extrusion limitations, Capillary heat transfer limit, Heat pipe manufacturing.

OLUK TASARIMINDA ÜRETİMSEL KISITLARIN ETKİSİ VE BUNUN ISI BORULARININ ISI TAŞIMA KAPASİTESİNİ BELİRLEMEDE KULLANILAN BİR ALGORTİMAYA UYGULANIŞI

Özet: Bu çalışmada, oluklu ısı boruları için maksimum ısı taşıma kapasitesinin hesaplamasına yönelik bir yöntem üzerinde durulmuştur. Yöntem, ekstrüzyon kısıtları, ısı borusu boyunca buhar ve sıvıda görülen basınç kayıplarına ek olarak buharlaştırıcı ve yoğuşturucu arasındaki sıcaklık düşüşünü de göz önünde bulundurmaktadır. Yöntemin bir algoritmaya uygulanışı ve öngörüsel başarımı, dikdörtgen, ikizkenar yamuk, ikizkenar üçgen ve girintili oluk şekillerine sahip ısı boruları için belli bir alan ve çalışma sıcaklığında gösterilmiştir. Bu çalışma sonucunda, girintili oluk tipinin diğer tiplere göre daha fazla ısı taşıma kapasitesine sahip olduğu görülmüştür.
Anahtar Kelimeler: Oluklu ısı borusu, Ekstrüzyon limitleri, Kılcal ısı transfer limiti, Isı borusu üretimi.

NOMENCLATURE

$\dot{m}$	Mass flow rate [kg/s]
$\bar{t}$	Average thickness [m]
A	Area [m^2]
c	Length of the constant thickness of the rim [m]
D	Diameter [m]
F	Force on a rim of a die [N]
f	Friction factor
g	Acceleration due to gravity [m/s^2]
h	Length of the variable thickness of the rim [m]
K	Permeability [m^2]
k	Thermal conductivity [W/m.K]
L	Length [m]
m	Mass [kg]
Ø	Groove angle [°]
P	Pressure [Pa]
Po	Poiseuille number [f.Re]
Q	Heat removal capacity [W]
r	Radius [m]
R	Resistance [°C/W]
Re	Reynolds number [=VρD/μ]
S	Safety factor
w	Width of the rim neck and the grooves [m]
δ	Groove depth [m]
ΔP	Pressure difference [Pa]
λ	Latent heat of vaporization [J/kg]
μ	Absolute viscosity [Pa.s]
ρ	Density [kg/m^3]
σ	Surface tension [N/m], stress [Pa]

Subscripts

a	adiabatic, axial
c	condenser, capillary
comp	compressive
e	evaporator
eff	effective
f	fin
h	hydraulic
i	inner, interface
l	liquid
max	maximum
o	outer
p	pipe

press	drum pressure
s	shear
sec	cross section
tot	total
ts	tensile
v	vapor
w	wick
y	yield

INTRODUCTION

For years, heat pipes have been widely used for thermal control in both terrestrial and celestial applications. The capability of transporting large amounts of heat between two terminals (evaporator and condenser) with a small temperature difference is the main characteristic of heat pipes which can be considered as an extra-high thermal conductivity device in the Fourier's law sense.

A conventional heat pipe (HP), which operates on a closed two-phase cycle, consists of a working fluid and a sealed container lined with a wicking material as shown in Fig. 1. To operate it, the container is evacuated and backfilled with just enough liquid to fully saturate the wick. When heat is applied along the evaporator section of a HP, the local temperature is raised slightly and part of the working fluid evaporates. This temperature difference results in a difference in vapor pressure which causes vapor to flow from the heated section to a cooler part of the pipe (condenser). The vapor condenses at the cooler part of the pipe and releases its latent heat. Return of the liquid condensate occurs through the wick as result of a capillary action.

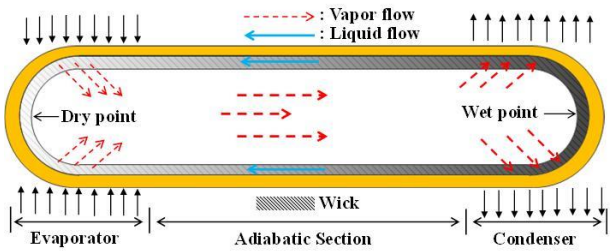

Figure 1. Working principle of a HP and its sections.

In the early studies, Babin et al. (1989) developed a simplified numerical model and conducted experiments for measuring the maximum heat transport rate of a micro HP which served as a foundation for subsequent researches. In one of these, Launay et al. (2004) developed a mathematical model for predicting the heat transport capacity and temperature distribution along the axial direction of a triangular heat pipe filled with water. A detailed evaporation and condensation model from kinetic theory was utilized and film thickness along evaporation and condensation micro regions were obtained, which were used to calculate thermal resistance and the heat transfer rate through the liquid film. Suman and Hoda (2005) on the other hand, studied the effect of contact angle, surface tension and viscosity of the working fluid, inclination, apex angle of V-groove, length of adiabatic section on the heat removal capacity of the heat pipe were studied.

In a different study, Lefevre et al. (2008) studied the heat conduction in each cross section in liquid and solid regions to obtain thermal resistances which were then used to find the axial temperature distribution along the heat pipe container with rectangular groves. The results were validated by experiments in which liquid-vapor interface radius and container temperatures were measured. An optimization study was carried out for maximum heat capacity as a function of groove height and width. In another investigation on rectangular grooved HPs, the effect of filling ratio and the vapor space thickness on thermal performance was investigated in a numerical and experimental study by Lips et al. (2010). It was shown that small vapor space induced liquid retention and thus reduced the thermal resistance of the system; however, it influenced the level of the liquid-vapor interface radii and hence reduced the maximum capillary pressure.

In addition to previous studies, Suh and Park (2003) completed a numerical analysis on thermal performance of flat micro-heat pipe with trapezoidal axial grooves considering the effect of interfacial shear stress. An outcome of the analysis is that the heat transport decreases with interfacial shear effect. In a different study, Kim et al. (2003) developed an analytical model for heat and mass transfer in a miniature heat pipe with trapezoidal grooves by taking into account the effect of liquid-vapor interfacial shear, contact angle, and the fluid inventory. The outcome of analysis was shown to be in close agreement with experimental results. It was also shown that the thermal performance of the heat pipe could be enhanced by numerical optimization of the grooves.

More recent studies on grove shapes focused on re-entrant (Ω) shape. Thomas and Damle (2005) proposed a good analysis on the fully developed laminar flow within a reentrant groove using a finite element model, and the capillary limit of a low-temperature heat pipe was also determined based on traditional capillary pressure balance. Later on, Chen et al. (2009) investigated the influence of variations in the capillary radius, liquid–vapor interfacial shear stress and the contact angle. The axial distribution of the capillary radius, fluid pressure and mean velocity are obtained.

Although an analysis with respect to vapor and liquid flow losses is compulsory and should be done in order to find the best groove geometry, it is not enough for a practical scenario which also includes of the fabrication phase of the HP. In most design activities, the manufacturing phase is often underestimated and production limitations are not taken into account. This leads to multiple iterations between the workshop and designer resulting in loss of time and money.

In this paper, a complementary but not alternative method is proposed which takes into account extrusion limits together with the vapor and liquid losses. By utilizing a mathematical model and algorithm presented by this study, one can understand that the groove design works and can be manufactured before going into the workshop. This paper is organized as follows; first the mathematical model and its implementation to an algorithm will be presented. Then predictive performance of the model together with the manufacturing limitations will be demonstrated on different groove geometries.

MATHEMATICAL MODELLING

The mathematical model employed in this study is based on the computation of maximum heat transfer capability by taking into account;

i. Manufacturing (extrusion) limitations on groove structure
ii. Maximum capillary pumping pressure
iii. Pressure drops along an HP and the gravitational head
iv. Temperature drop (criteria) between the evaporator and the condenser

The Effect of Extrusion Limits on Groove Structure

Extrusion is the manufacturing process of axially groove heat pipes. It utilizes a plastic deformation process in which a block of metal (billet) is forced to flow by compression through the die opening of a smaller cross-sectional area than that of the original billet.

In Fig. 2, a die used for the manufacturing of a re-reentrant grooved HP is shown. As billet flows through rims of the die, the grooves of a HP are formed. In order to form such narrow grooves, the rims of the die should be able to withstand high compressive forces (shown by the red arrows) during an extrusion process. If the neck of a die is too narrow, the force applied during the extrusion may break the neck and the shape of grooves will be ruined.

In Fig. 3, a single rim is demonstrated. As can be seen, the rim is thick at the beginning (with respect to flow direction) and stays constant for a section and it gets thinner towards to the end of the die.

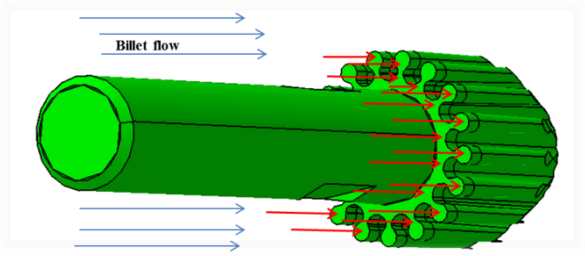

Figure 2. A die for manufacturing re-reentrant grooved HP.

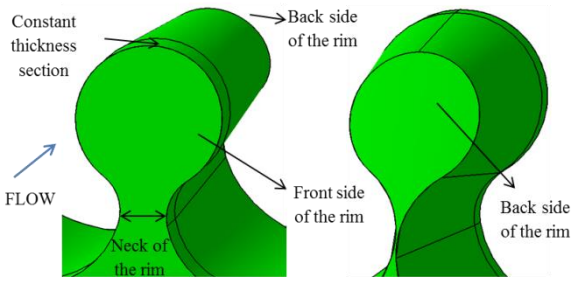

Figure 3. Front and back view of a rim

If section view is taken from the narrowest part of a rim, it looks like a triangle which is shown in Fig. 4. If the tensile strength of the die is not high enough to withstand shear forces created at this triangular area of the rim, the rim will be torn from this section. The analysis is based on the following expression.

$$F_{comp,net} \leq F_{yield,shear} \quad (1)$$

where $F_{comp,net}$ is the net force resulting from compressive normal pressure to front face (Ω) of the rim (shaded with black lines), $F_{yield,shear}$ is the yield shear force of the rim defined as the the tensile stress (σ_{ts}) of the die material times the sectional area, A_{sec}, where the shear stress is applied (shaded by yellow and green). As can be seen in the Fig. 4, A_{sec} can be found by adding the triangle area to the rectangle area which can be expressed as;

$$A_{sec} = \frac{w\,h}{2} + \mathrm{w}\,c \quad (2)$$

where w is the width of the neck (at the same time the groove width), c is the length of the rim where the thickness is not changed, h is length of the rim where the thickness is changing. In most of the die designs, there is 1 degree inclination (Bauser et al. 2006) after the constant thickness portion. h can be computed by determining of the point where the edges of the triangle intersect,

$$h = \tan(1^{\circ}) + \frac{w}{2} \quad (3)$$

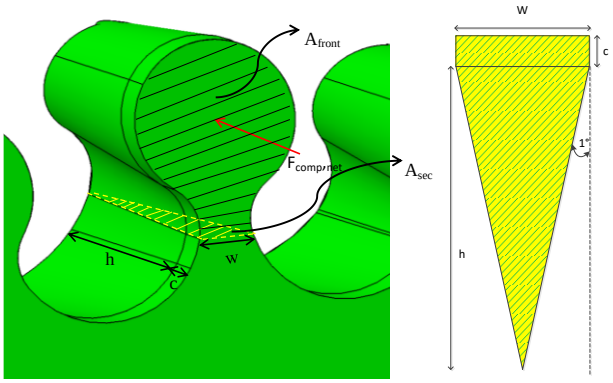

Figure 4. Characteristic dimensions of the rim

To find $F_{comp,net}$, below equation is used,

$$F_{comp,net} = A_{front}\, S\, P_{press} \quad (4)$$

where A_{front} is the area where compressive forces are applied, S is the safety factor which is at most 1.5 [Bauser et al., 2006, Saha, 2006) to find maximum extrusion load, P_{press} is the compressive pressure applied by the ram.

Consequently, as long as the Eq. 1 is fulfilled, an extrusion process can be performed without any rupture. It should carefully be noted that, the change of the width of the neck affects A_front and A_sec which eventually affects the compressive net force applied to front face of the rim and the shear force applied to the area where the section view is taken.

The Maximum Capillary Pumping Pressure

During steady state operation, to find the maximum capillary pumping pressure, it can be assumed that the effective capillary radius at the wet point, $r_{c,c}$, approaches to infinity where the contact angle (Reay and Kew, 2013) is equal to 90°, whereas at the dry point it is equal to 0° which yields the maximum capillary pumping pressure as follows (Reay and Kew, 2013)

$$\Delta P_{c,max} = \frac{2\sigma}{r_{c,e}} \quad (5)$$

The effective capillary radius for some of the common groove shapes recommended by Zohuri (2016) and Brennan et al. (1979) are listed in Table 1.

Table 1. Effective Capillary Radius for Some of the Common Groove Shapes (Zohuri, Brennan et al.)

Groove type	Effective capillary radius
Rectangular	w
Triangular	w/(cos Ø/2)
Trapezoidal	w
Re-entrant	w

Vapor Pressure Drop

The variation of vapor pressure is principally the result of the viscous pressure drop occurring along the vapor flow path. If one-dimensional vapor pressure drop expression presented by Zohuri (2016) is used, the vapor pressure drop can be expressed as follows

$$\Delta P_v = \left(\frac{(f_v Re_v)\mu_v}{2(r_{h,v})^2 A_v \rho_v \lambda}\right) L_{eff} Q_{max} \quad (6)$$

where f_v is the friction factor of the vapor, Re_v is the Reynolds number of vapor, μ_v is the absolute viscosity of vapor, $r_{h,v}$ is the hydraulic radius of the vapor space, A_v is the cross sectional area of the vapor, ρ_v is the vapor density, λ is latent heat of vaporization, Q_{max}, is the maximum heat removal capacity of the HP, L_{eff} is the effective length of the HP.

Since mass flow will vary in both the evaporator and the condenser region, an effective length rather than the geometrical length must be used for these regions. If the mass change per unit length is constant, the total mass flow will increase or decrease, linearly along the regions. Therefore, the lengths of the evaporator L_e and the condenser L_c can be replaced by $L_e/2$ and$L_c/2$. The total effective length, L_{eff} , for fluid flow will then be expressed as,

$$L_{eff} = L_a + \frac{L_e + L_c}{2} \quad (7)$$

where L_a is the length of adiabatic section.

During steady state operation, the liquid mass flow rate at any axial position, $\dot{m}_l$, must be equal to the vapor mass flow rate, $\dot{m}_v$,and while the liquid regime is always laminar, the vapor flow may be laminar or turbulent. Therefore it is necessary to determine the vapor flow regime as a function of the heat input. This can be done by evaluating axial Reynolds number in the vapor phase as,

$$Re_v = \frac{2\,\dot{m}}{\pi r_v \mu_v} \quad (8)$$

relating the heat and mass flows as, $Q_{max} = \dot{m}_v \lambda$, Reynolds number of the vapor phase becomes,

$$Re_v = \frac{2\,(r_{h,v})\,Q_{max}}{\lambda\, A_v\, \mu_v} \quad (9)$$

Depending on the Reynolds number, the following correlations could be used with reasonable accuracy (Zohuri, 2016)

$$Re_v < 2300 \quad (f_v Re_v) = 16 \quad (10)$$

$$Re_v > 2300 \quad (f_v Re_v) = 0.038\left(\frac{2\,(r_{h,v})\,Q_{max}}{\lambda\, A_v\, \mu_v}\right)^{0.75} \quad (11)$$

Liquid Pressure Drop

Like in vapor phase, viscous forces in the liquid also results in a pressure drop. For constant heat addition and removal, this liquid pressure drop can be calculated from the following [13],

$$\Delta P_l = \frac{L_{eff}\, \mu_l\, Q_{max}}{K A_w\, \rho_l\, \lambda} \quad (12)$$

where μ_l is the absolute viscosity of liquid, ρ_l is the liquid density, A_w is the cross sectional area of the wick, K is the permeability which can be introduced as

$$K = \frac{2\,\epsilon\,(r_{h,l})^2}{f_l Re_l} \tag{13}$$

where ϵ is the porosity which is equal to 1, $r_{h,l}$ is the hydraulic radius of the liquid flow passage, $f_l Re_l$ is the product of Reynolds number and the friction factor of the liquid. In the literature, this product may also be named as Poiseuille number (Po). While it is independent of the flow path, it is strongly and only dependent upon the shape of the flow passage which is in this case the groove geometry. Although Poiseuille number for rectangular and annular flow passages can be found easily in various sources (Zohuri,2013), it is rather difficult work to find Poiseuille number for arbitrary passages.

There are several approaches (Thomas and Damle, 2005; Muzychka and Yovanovicht, 2004; Shah , 1975) to find Poiseuille number for arbitrary passages. In the present investigation for isosceles triangular, rectangular and trapezoidal passages (groove shapes), the approach suggested by Shah (1975) will be used, whereas for the re-entrant (Ω) groove, the method of Thomas and Damle (2005) will be utilized. In Fig. 5, the alternative groove shapes and their parameters which will be used to find non-dimensional parameters are shown.

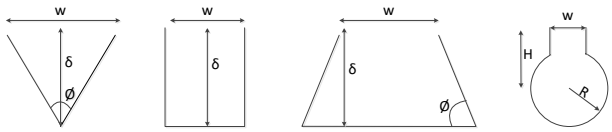

Figure 5. The groove shapes and parameters.

The Gravitational Head

At 1-g conditions, the gravitational head can be written as (Vlassov et al., 2008);

$$\Delta P_g = \rho_l\, g\, l\, sin\emptyset + \rho_l\, g\, \delta \tag{14}$$

where ρ_l is the liquid density, g is the acceleration due to gravity, l is the heat pipe length , δ is the groove depth and $\emptyset$ is the angle between the heat pipe and the horizontal ($\emptyset$ is positive when the condenser is lower than the evaporator).

Governing Equation for Maximum Heat Transport Rate

For a proper operation of a heat pipe, the maximum capillary pumping pressure, ΔPc,max , must be greater than the total pressure drop along the pipe which can be expressed as

$$\Delta P_{c,max} \geq \Delta P_l + \Delta P_v + \Delta P_g \tag{15}$$

where $\Delta P_{c,max}$ is the maximum capillary pumping pressure generated within groove structure between evaporator and the condenser, ΔP_l is pressure drop occurring in the liquid phase, ΔP_v, pressure drop occurring in the vapor phase, ΔP_g the pressure drop due to the gravitational head (which may be zero, positive or negative, depending on the inclination of the heat pipe).

If the Eq. (15) is not met, the working fluid will not returned to the evaporator, the wick will dry out in the evaporator region and the heat pipe will not operate. The maximum allowable heat flux for which Eq. (15) holds is referred to as the capillary heat transfer limit. If Eq. (5), Eq. (6), Eq. (12), Eq. (14) are substituted into Eq. (15), the transport capacity can be found as a function of effective length,

$$Q_{max}\, L_{eff} = \frac{\frac{2\sigma}{r_{c,e}} - (\rho_l\, g\, l\, sin\emptyset + \rho_l\, g\, \delta)}{\left(\frac{(f_v Re_v)\mu_v}{2(r_{h,v})^2 A_v \rho_v\, \lambda} + \frac{\mu_l}{K A_w\, \rho_l\, \lambda}\right)} \tag{16}$$

Methodology for the Determination of Temperature Drop between Evaporator and Condenser

Temperature drop between evaporator and condenser of a HP is another important figure-of-merit and of particular interest to the designer. To evaluate temperature drop, thermal network method stems from electrical analogy (Kotcioğlu et al., 2009) is utilized. HP can be represented with the following network of resistances (Fig. 6):

- $R_{p,e}$:Radial resistance of the pipe wall at the evaporator
- $R_{w,e}$: Resistance of the liquid-wick combination at the evaporator
- $R_{i,e}$: Resistance of the liquid-wick interface at the evaporator
- $R_{v,a}$: Axial resistance of the vapor section
- $R_{p,a}$: Axial resistance of the pipe wall
- $R_{w,a}$: Axial resistance of the liquid-wick combination
- $R_{i,c}$: Resistance of the liquid-wick interface at the condenser
- $R_{w,c}$: Resistance of the liquid-wick combination at the condenser
- $R_{p,c}$:Radial resistance of the pipe wall at the condenser

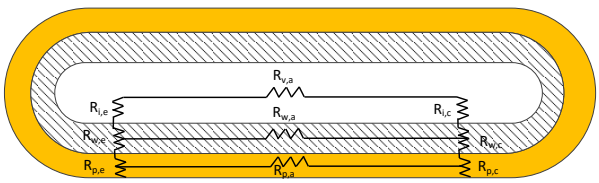

Figure 6. The thermal resistances of a HP.

The order of magnitude for each resistance was investigated by Asselman and Green (1982) and the estimates for each resistance are given in Table 2.

When the values are compared, it is apparently seen that several simplifications can be made. Firstly, due to the comparative magnitudes of $R_{v,a}$, $R_{p,a}$ and $R_{w,a}$, the overall resistance network can be simplified to Eq. (17).

$$R_{tot} = R_{p,e} + R_{w,e} + R_{i,e} + R_{v,a} + R_{i,c} + R_{w,c} + R_{p,c} \quad (17)$$

Table 2. Comparative values for HP resistance (Asselman and Green, 1982).

Resistances	°C/W
$R_{p,e}$ and $R_{p,c}$	10^{-1}
$R_{w,e}$ and $R_{w,c}$	10^{+1}
$R_{i,e}$ and $R_{i,c}$	10^{-5}
$R_{v,a}$	10^{-8}
$R_{p,a}$	10^{+2}
$R_{w,a}$	10^{+4}

Secondly, if magnitudes of $R_{i,e}$, $R_{i,c}$, $R_{v,a}$ are compared with $R_{p,e}$, $R_{p,c}$,$R_{w,e}$, $R_{w,c}$, the terms $R_{i,e}$, $R_{i,c}$, $R_{v,a}$ can be assumed to be negligible which yields the total resistance as,

$$R_{tot} = R_{p,e} + R_{w,e} + R_{w,c} + R_{p,c} \quad (18)$$

The radial resistance at the pipe wall can be calculated by applying Fourier's law as

$$R_{p,e} = \frac{\ln\left(D_o/D_i\right)}{2\pi L_e k_p} \quad (19)$$

$$R_{p,c} = \frac{\ln\left(D_o/D_i\right)}{2\pi L_c k_p} \quad (20)$$

where D_o and D_i are the outer and inner diameters of the HP, respectively (Fig. 7).

The most complicated and difficult to find resistance is liquid-wick combination resistances which is frequently a very significant contributor to the overall resistance. The best approach is to use measured values wherever possible. So, for this resistance, an experimentally obtained film coefficients, accounts for the conductance through the liquid-wick combination at evaporator and the condenser sections suggested by Kamotani (1978) are utilized. As a result, the liquid-wick combination resistances can be expressed by

$$R_{w,e} = \frac{0.0701 + \frac{k_l \delta}{k_p \overline{t_f}}}{N k_l L_e} \quad (21)$$

$$R_{w,c} = \frac{0.0221 + \frac{k_l \delta}{k_p \overline{t_f}}}{N k_l L_c} \quad (22)$$

where k_l is the liquid thermal conductivity, k_p is the wall thermal conductivity, δ is the groove depth, $\overline{t_f}$ is the average fin thickness , N is the total number of grooves (see Fig. 7).

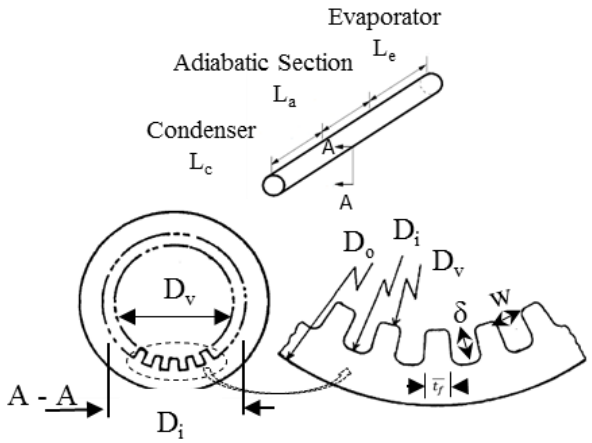

Figure 7. The characteristic dimensions of an HP.

Finally, the total resistance can be expressed as

$$R_{tot} = \frac{\ln\left(D_o/D_i\right)}{2\pi L_e k_p} + \frac{\ln\left(D_o/D_i\right)}{2\pi L_c k_p} + \frac{0.0701 + \frac{k_l \delta}{k_p \overline{t_f}}}{N k_l L_e} + \frac{0.0221 + \frac{k_l \delta}{k_p \overline{t_f}}}{N k_l L_c} \quad (23)$$

Applying Ohm's law, the temperature drop between evaporator and condenser can be found by the following expression

$$\Delta T = Q_{max} R_{tot} \quad (24)$$

ALGORITHM TO FIND CAPILLARY HEAT TRANSFER LIMIT OF THE GROOVED HEAT PIPES

As examined in aforementioned sections, the width of the die neck (which is actually the width of manufactured groove) determines the characteristic forces on the rim. Additionally, it also dictates the maximum capillary pumping pressure and affects liquid pressure drop. Likewise the width of a groove, the depth of the groove also affects the liquid pressure drop and the net forces on the rim. Thus, a groove shape optimization should be done not only with respect to vapor and liquid flow losses, but also with respect to extrusion limitations. The implementation of the mathematical model together with the manufacturing limits into an algorithm is shown in Fig. 8.

PREDICTION PERFORMANCE OF THE MATHEMATICAL MODEL

The performance of the mathematical model will be demonstrated in comparison experimental results of Chen et al. (2009) on re-entrant grooved HP and the study of Kim et al. (2003) on trapezoidal grooved HP. The geometric parameters of the HPs used in those studies are given in Table 3. The model predictions and experimental results for two different groove types are shown in Fig. 10.

An overall inspection of profiles reveals that the predictions agree reasonably well with the test data (maximum average error is 15.1 %). On the other hand, it is also seen that the capillary heat transfer limits are over predicted. This is attributed to the fact that the interfacial shear stress between vapor and liquid is neglected in the model:

Secondly, in order to verify the model for the temperature drop between the evaporator and the condenser, again the study of Kim et al. (2003) on trapezoidal grooved HP is utilized. In Table 4, some model predictions are given in comparison with the experiment results of Kim *et al.* (2003). It is seen that the model results slightly over-predicted due to the over prediction of capillary heat transfer limits (see Eq. 24) and neglecting some of the resistance in the model.

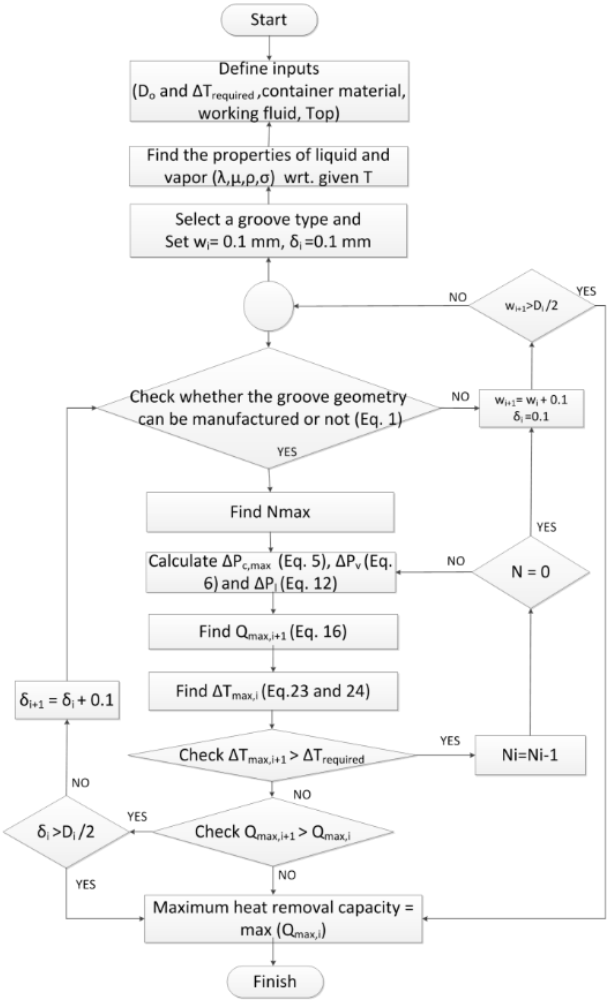

Figure 8. Flowchart to find maximum capillary heat transfer limit.

Table 3. Geometric parameters of grooved HPs in the studies of Chen et al.(2009) and Kim et al. (2003).

	Re-entrant	Trapezoidal
Working fluid	ammonia	water
Evaporator section length (m)	0.7	0.1
Adiabatic section length (m)	0.56	0.1
Condenser section length (m)	0.59	0.095
External diameter (m)	0.0125	0.003
Diameter of a groove (m)	0.0014	-
Angle of a groove (°)	-	84
Width of a groove (m)	0.00046	0.000123
Depth of a groove (m)	0.00207	0.000131
Number of groove	15	26
Adverse tilt angle	0	0

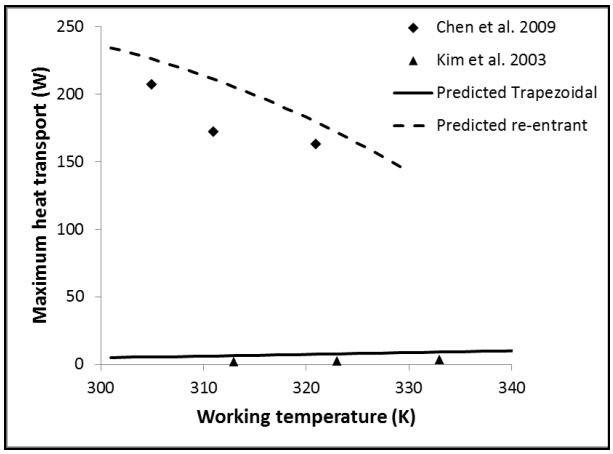

Figure 9. Comparison of the predictive maximum heat transport with the experimental data.

Table 4. Comparison of the predictive temperature drop with the experimental data.

$T_{operation}$ (K)	313	323	333
ΔT_{exp}	0.33	0.31	0.37
$\Delta T_{predict}$	0.40	0.48	0.55

RESULTS AND DISCUSSION

In this section heat removal performance of different groove geometries will be presented. Test problem and characteristics of the HP are as follows:

- The evaporator, adiabatic, condenser lengths are selected as 333.3, 666.6, 333.3 mm respectively which makes Leff equal to1 meter.
- The wall thicknesses of the HP and Di are selected as 1.15, 10.2 mm, respectively.
- DIN 2344 tool steel having a tensile strength of 900 N/mm2 at 500 C° is chosen for the die material
- The working fluid and the container material are selected as ammonia and 6063-T6 aluminum alloy, respectively.
- The temperature difference criterion (ΔT) between evaporator and condenser is defined as 10K.
- The HP operating temperature is 293 K.
- The HP is filled with just enough liquid to fully saturate the wick (i.e. enough mass to fill the grooves completely with liquid and vapor volume with vapor.)

For above specifications, heat removal capacities (at 0-g) of isosceles triangular, rectangular, trapezoidal, re-entrant type grooved HPs are found by executing the algorithm and presented in Tables 5-8. While performing the simulations, increments in all dimensions (width, depth and diameter) are taken as 0.1 mm due to the limitations imposed by the current level of extrusion devices. One can expect to obtain numerous combinations of operable heat pipes (for each groove geometry) which can meet above assumptions. However, in this paper, representative cases which help the authors demonstrate the general trends will be presented. At the end of each groove geometry, the optimum case with the highest capillary heat transfer limit will also be presented.

When the results obtained for rectangular groove (Table 5) are examined, it can be said that for narrow groove widths, the maximum capillary pumping pressure is higher. However, for narrow widths (0.1 – 0.2 mm) when depth is high (17 - 20 times of the width), compressive force on the rims of a die approaches to yield shear forces which brings difficulties in manufacturing. On the other hand, when the depth increases while keeping width the same, the hydraulic
radius, Poiseuille number, the total wick area increase. Combined effect of this is in an increment in the capillary heat transfer limit. Additionally, this increase in depth results in an escalation of the temperature difference between evaporator and condenser. This escalation stems from the increase of the liquid volume in grooves leading to higher resistance of the liquid-wick combination. Furthermore, as expected, if the number of grooves increases while the width and depth of the groove remains same, the capillary heat transfer limit increases, but as a drawback, the temperature difference between evaporator and condenser also increases. Thus, while increasing depth and the groove number, not only the manufacturing limits but also the temperature difference between evaporator and condenser limitation also should be taken into consideration, otherwise HP cannot work since the required temperature difference will be higher than the temperature difference supplied by the environment. Overall, the best configuration is obtained for case 8 which has the highest capillary heat transfer limit while obeying temperature difference and manufacturing limitations.

Results obtained for the triangular groove are presented in Table 6. They exhibit similar behavior with those obtained for rectangular groove. On the whole, the capillary heat transfer performance of the triangular grooves is less than the rectangular ones and they are disadvantageous in terms of mass also.

In Table 7, the predictions obtained for the trapezoidal grooves are presented. When the width and the depth are kept small (~0.1 - 0.2 mm), increasing the wall angle results in a decrease in the capillary heat transfer limit (see cases 1-3). Whereas when the depth is increased keeping width constant, the angle increase results in an increment of the capillary heat transfer limit. This is

Table 5. The predictions for rectangular grooves.

	Case 1	Case 2	Case 3	Case 4	Case 5	Case 6	Case 7	Case 8	Case 9
Width of a groove (mm)	0.10	0.20	0.40	0.40	1.00	1.00	1.00	1.10	1.20
Depth of a groove (mm)	1.70	3.00	0.70	0.80	1.00	1.00	1.00	1.10	1.00
Number of groove	105	43	54	54	12	23	22	20	18
$\Delta P_{c,max}$ (Pa)	456.96	228.48	114.24	114.24	45.7	45.7	45.7	41.54	38.08
$F_{comp,net}$ (kN)	0.17	0.59	0.27	0.31	0.98	0.98	0.98	1.18	1.17
$F_{yield,shear}$ (kN)	0.17	0.61	2.24	2.24	13.34	13.34	13.34	16.09	19.1
Total mass (g/m)	195.97	240.00	135.52	138.38	163.67	140.67	142.76	145.04	143.60
Q_{max} (W)	28.12	76.97	89.33	104.82	134.63	250.23	240.01	279.16	246.38
ΔT (K)	0.26	1.56	1.23	1.49	6.59	7.54	7.32	9.4	8.83

Table 6. The predictions for triangular grooves.

	Case 1	Case 2	Case 3	Case 4	Case 5	Case 6	Case 7	Case 8	Case 9	Case 10
Width of a groove (mm)	0.30	1.10	1.20	1.20	1.30	1.40	1.60	1.90	2.00	2.10
Depth of a groove (mm)	1.60	1.60	1.60	1.70	1.70	1.70	1.70	1.90	2.00	2.20
Ø (°)	10.71	37.94	41.11	38.88	41.85	44.76	50.40	46.11	53.13	51.03
Number of groove	54	18	16	16	15	14	12	9	9	8
$\Delta P_{c,max}$ (Pa)	151.65	39.29	35.66	35.91	32.83	30.18	25.84	22.08	20.44	19.64
$F_{comp,net}$ (kN)	0.23	0.86	0.94	0.99	1.08	1.16	1.33	2.04	1.95	2.25
$F_{yield,shear}$ (kN)	1.30	16.09	19.10	19.10	22.37	25.89	33.72	47.39	52.46	57.79
Total mass (g/m)	200.34	194.32	195.32	199.17	198.64	198.46	199.17	220.68	212.20	221.37
Q_{max} (W)	28.43	98.27	99.91	107.26	113.02	117.04	119.79	137.78	137.09	135.61
ΔT (K)	0.39	3.40	3.83	4.14	4.63	5.10	6.01	9.16	9.07	10.06

due to the fact that the volume for a single groove is increased and more grooves can be manufactured within the allowable space. On the other hand, when large widths are attempted, although the capillary heat transfer limit increases the temperature difference criterion between the evaporator and the condenser is violated (case 10). The best groove configuration is obtained in Case 5 having 85° for which the capillary heat transfer limit is 382.02 W.

The final set of results to be presented within the scope of this paper is of re-entrant type (Table 8). As expected, combination of small widths with large diameters yields to high heat transfer limit. However, after a certain point, selecting large diameters leads to high compressive forces, which in turn leads to manufacturing difficulties (Cases 1-4). Furthermore, one would expect that increasing the depth while keeping the width and diameter constant results in increasing heat transport capacity (Cases 1-4) as observed for rectangular grooves (Table 5) . However, this trend is not necessarily true for re-entrant grooves as seen in Cases 5-8. The explanation of this phenomenon lies in the fact that hydraulic radius is directly proportional with depth for rectangular groves but indirectly proportional with depth for re-entrant grooves which effects Poiseuille number (see appendix), wick area and therefore heat transfer capacity. When width is equal to 0.3 mm, the best capillary heat transfer limit is achieved (case 5). Increasing the width after this point, the heat removal performance starts to decrease. Moreover, higher widths (=>1.1 mm) violate the temperature difference criterion (Case 10).

In Fig. 10, maximum heat transfer capacities obtained for each groove type is plotted with respect to temperature. It is seen that re-entrant groove type exhibits the best performance throughout the entire temperature range. Moreover, highest heat transfer capacities for all groove types are obtained in the range of 280-290 K. This due to the fact that the liquid transport factor (LTF) of ammonia defined in (Brennan et al., 1979) is highest in this range.

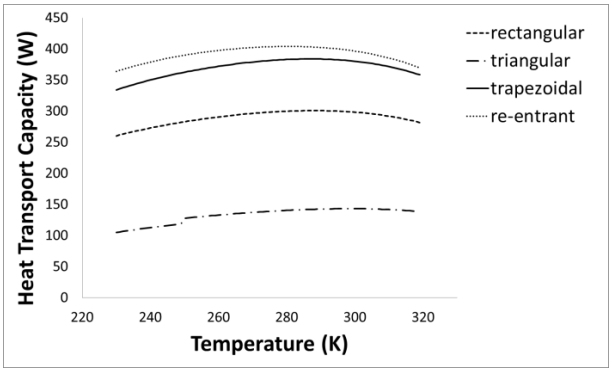

Figure 10. The predicted maximum heat transport capacities for different operating temperatures

Table 7. The predictions trapezoidal grooves.

	Case 1	Case 2	Case 3	Case 4	Case 5	Case 6	Case 7	Case 8	Case 9	Case 10
Ø (°)	30	75	75	85	85	85	86	87	85	85
Width of a groove (mm)	0.10	0.10	0.20	0.20	0.30	0.30	0.30	0.30	0.40	1.10
Depth of a groove (mm)	0.20	0.20	1.10	1.70	2.00	2.10	2.10	2.60	2.20	1.60
Number of groove	35	102	35	53	41	37	45	39	18	18
$\Delta P_{c,max}$ (Pa)	456.96	456.96	228.48	228.48	152.32	152.32	152.32	152.32	114.24	41.54
$F_{comp,net}$ (kN)	0.09	0.03	0.53	0.58	0.93	0.99	0.91	1.11	1.27	1.93
$F_{yield,shear}$ (kN)	0.17	0.17	0.61	0.61	1.30	1.30	1.30	1.30	2.24	16.09
Total mass (g/m)	121.15	121.13	155.81	167.60	168.41	176.43	166.73	185.85	210.96	152.78
Q_{max} (W)	11.34	7.95	288.20	301.93	382.02	375.55	369.12	324.89	265.94	404.76
ΔT (K)	0.19	0.05	5.69	5.33	9.19	9.13	9.27	8.63	9.66	17.00

Table 8. The predictions for re-entrant grooves.

	Case 1	Case 2	Case 3	Case 4	Case 5	Case 6	Case 7	Case 8	Case 9	Case 10
Diameter of a groove (mm)	0.40	0.40	0.80	0.80	1.00	1.00	1.00	1.00	1.00	1.10
Width of a groove (mm)	0.10	0.10	0.20	0.20	0.30	0.30	0.30	0.40	0.40	0.30
Depth of a groove (mm)	0.40	0.80	0.80	1.30	1.00	1.10	2.40	1.00	2.00	1.10
Number of groove	61	61	32	32	26	26	26	26	26	23
$\Delta P_{c,max}$ (Pa)	456.96	456.96	228.48	228.48	152.32	152.32	152.32	114.24	114.24	152.32
$F_{comp,net}$ (kN)	0.12	0.16	0.49	0.59	0.77	0.80	1.18	0.77	1.16	0.93
$F_{yield,shear}$ (kN)	0.17	0.17	0.61	0.61	1.30	1.30	1.30	2.24	2.24	1.30
Total mass (g/m)	127.92	153.35	140.82	168.49	145.94	151.18	203.87	145.77	185.10	149.83
Q_{max} (W)	74.03	77.26	307.03	309.40	401.17	398.41	348.09	318.13	331.86	498.21
ΔT (K)	0.80	0.89	6.11	6.47	9.82	9.84	9.60	7.87	9.01	13.64

CONCLUSIONS

In this paper, a mathematical model for the computation of maximum heat transfer capability of grooved HPs was presented. The model embodies the pressure drops in liquid and vapor phases as well as the manufacturing limitations imposed by the current state of the art of extrusion technology. The model was implemented to an algorithm and its predictive performance was demonstrated on different groove geometries. The conclusions drawn at the end of this study are as follows:

- For small widths (~0.1 - 0.2 mm.), when the depths are higher (17-20 times of the width for rectangular grooves, 6-8 times of the width for trapezoidal and re-entrant grooves), compressive forces on the rims of the die approaches to yield shear forces which imposes manufacturing difficulties.

- If the number of grooves increases while the width and depth of the groove remains same, the capillary heat transfer limit increases, but as a drawback, the temperature difference between evaporator and condenser also increases.

- For a specific allowable space and working temperature, the best HPs performance is achieved by the re-entrant type grooved HP.

- Among the groove configurations examined in this study, rectangular grooves leads to lightest heat pipes (mass) for a specific allowable space which makes this groove type a viable choice for mass sensitive applications.

- Triangular grooves leads to heat pipes with worst performance for all configurations since it has the highest mass and the least heat transport performance.

APPENDIX

Isosceles Triangular Groove

$$1 < \frac{\delta}{w} < 8 \qquad Po = 13{,}7269 - 0{,}4462\left(\frac{\delta}{w}\right) + 0{,}0527\left(\frac{\delta}{w}\right)^2 - 0{,}0023\left(\frac{\delta}{w}\right)^3$$

Rectangular Groove

$$0 < \frac{w}{\delta} \le 1 \qquad Po = 23{,}9971 - 32{,}1146\left(\frac{w}{\delta}\right) + 42{,}6604\left(\frac{w}{\delta}\right)^2 - 28{,}5012 + 8{,}1857\left(\frac{w}{\delta}\right)^4$$

Trapezoidal Groove

For $\emptyset = 85$;

$$1.333 < \frac{\delta}{w} < 8 \qquad Po = 12{,}7818 + 1{,}1930\left(\frac{\delta}{w}\right) - 0{,}0263\left(\frac{\delta}{w}\right)^2 - 0{,}0062\left(\frac{\delta}{w}\right)^3$$

$$0.125 < \frac{w}{\delta} \le 1.333 \qquad Po = 23{,}9026 - 31{,}3020\left(\frac{\delta}{w}\right) + 42{,}8845\left(\frac{\delta}{w}\right)^2 - 32{,}8690\left(\frac{\delta}{w}\right)^3 + 14{,}3776\left(\frac{\delta}{w}\right)^4 - 2{,}7577\left(\frac{\delta}{w}\right)^5$$

For $\emptyset = 75$;

$$1.333 < \frac{\delta}{w} < 8 \qquad Po = 13{,}7220 + 0{,}2540\left(\frac{\delta}{w}\right) + 0{,}0407\left(\frac{\delta}{w}\right)^2 - 0{,}0067\left(\frac{\delta}{w}\right)^3$$

$$0.125 < \frac{\delta}{w} \le 1.333 \qquad Po = 23{,}8591 - 31{,}7212\left(\frac{\delta}{w}\right) + 47{,}1704\left(\frac{\delta}{w}\right)^2 - 40{,}8044\left(\frac{\delta}{w}\right)^3 + 19{,}8817\left(\frac{\delta}{w}\right)^4 - 4{,}1337\left(\frac{\delta}{w}\right)^5$$

For $\emptyset = 60$;

$$1.333 < \frac{\delta}{w} < 8 \qquad Po = 14{,}3651 - 0{,}5443\left(\frac{\delta}{w}\right) + 0{,}1558\left(\frac{\delta}{w}\right)^2 - 0{,}0119\left(\frac{\delta}{w}\right)^3$$

For $\emptyset = 45$;

$$2 < \frac{\delta}{w} < 8 \qquad Po = 13{,}4250 - 0{,}0355\left(\frac{\delta}{w}\right) + 0{,}0025\left(\frac{\delta}{w}\right)^2$$

$$0.25 < \frac{\delta}{w} \le 2 \qquad Po = 22{,}1641 - 26{,}7398\left(\frac{\delta}{w}\right) + 36{,}8631\left(\frac{\delta}{w}\right)^2 - 27{,}1792\left(\frac{\delta}{w}\right)^3$$

For $\emptyset = 30$;

$$0.125 \le \frac{\delta}{w} \le 8 \qquad Po = \frac{27{,}5886 + 131{,}8860\left(\frac{\delta}{w}\right)}{1 + 11{,}0425\left(\frac{\delta}{w}\right) - 0{,}0767\left(\frac{\delta}{w}\right)^2}$$

Re-entrant Groove

For $\left(\frac{H}{R} = 1\right)$;

$$0.1 \le \frac{w}{2R} \le 0.9 \qquad Po = 16{,}3943 + 7{,}7687\left(\frac{w}{2R}\right) - 4{,}1797\left(\frac{w}{2R}\right)^2 - 16{,}8051\left(\frac{w}{2R}\right)^3 + 22{,}1635\left(\frac{w}{2R}\right)^4 - 8{,}1793\left(\frac{w}{2R}\right)^5$$

For $\left(\frac{H}{R} = 2\right)$;

$$0.1 \le \frac{w}{2R} \le 0.9 \qquad Po = 9{,}2817 + 23{,}2370\left(\frac{w}{2R}\right) + 125{,}2087\left(\frac{w}{2R}\right)^2 - 357{,}2655\left(\frac{w}{2R}\right)^3 + 50{,}7287\left(\frac{w}{2R}\right)^4 - 6{,}9649\left(\frac{w}{2R}\right)^5$$

For $\left(\frac{H}{R} = 3\right)$;

$$0.1 \le \frac{w}{2R} \le 0.9 \qquad Po = 6{,}1287 + 17{,}2543\left(\frac{w}{2R}\right) + 159{,}1925\left(\frac{w}{2R}\right)^2 - 399{,}4492\left(\frac{w}{2R}\right)^3 + 344{,}0246\left(\frac{w}{2R}\right)^4 - 102{,}3792\left(\frac{w}{2R}\right)^5$$

REFERENCES

Asselman G. A. A. and Green D. B., 1982, *Heat Pipes, Phillips Technical Review*, 16, 169-186.

Babin B.R., Peterson G.P. and Wu D., 1989, Analysis and testing of a micro heat pipe during steady-state operation, *Proceedings of ASME/AIChE National Heat Transfer Conference*, 89-HT-1, Philadelphia, Pennsylvania.

Bauser M., Sauer G. and Siegert K., 2006, *Extrusion* (2nd Ed.). ASM International, Ohio.

Brennan J.P. and Kroliczek E. J., 1979 *Heat Pipe Design Handbook*, Volume 1, B&K Engineering, Maryland.

Chen Y., Zhang C., Shi M., Wua J. and Peterson G.P., 2009, Study on flow and heat transfer characteristics of heat pipe with axial ''Ω"-shaped microgrooves, *International Journal of Heat and Mass Transfer*, 52, 636–643.

Kamotani Y., 1978, Evaporator film coefficients of grooved heat pipes, *3rd International Heat Pipe Conference.*

Kim S. J., Seo, J. K., and Do, K. H., 2003, Analytical and Experimental Investigation on the Operational Characteristics and the Thermal Optimization of a Miniature Heat Pipe with a Grooved Wick Structure, *International Journal of Heat and Mass Transfer*, 43, 2051–2063.

Kotcioğlu İ., Çalışkan S. and Manay E., 2009, Cooling of a CPU with heat pipes using different refrigeration fluids, *J. of Thermal Science and Technology*, 29, 2, 109-116.

Launay S., Sartre V. and Lallemand M., 2004, Hydrodynamic and thermal study of a water-filled micro-heat-pipe array, *Journal of Thermophysics and Heat Transfer*, 18(3), 358-363.

Lefèvre F., Rullière R., Pandraud G. and Lallemand M., 2008, Prediction of the temperature field in at plate heat pipes with micro-grooves-experimental validation. *International Journal of Heat and Mass Transfer*, 51, 4083-4094.

Lips S., Lefèvre F. and Bonjour J., 2010, Combined effects of the filling ratio and the vapor space thickness on the performance of a flat plate heat pipe, *International Journal of Heat and Mass Transfer*, 53, 694-702.

Muzychka Y.S. and Yovanovicht M.M., 2004, Laminar Forced Convection Heat Transfer in the Combined Entry Region of Non-Circular Ducts, *Transactions of the ASME*, 126, 54-61.

Muzychka, Y. S. and Yovanovich M. M., 2002, Laminar Flow Friction and Heat Transfer in Non-Circular Ducts and Channels: Part I—Hydrodynamic Problem, *Compact Heat Exchangers: A Festschrift on the 60th Birthday of Ramesh K. Shah*, Grenoble, France.

Reay D. and Kew P., 2013, *Heat Pipe Theory, Design and Applications* (6th Ed.), Butterworth-Heinemann, MA.

Saha P. K., 2002, *Aluminum Extrusion Technology*, ASM International, Ohio.

Shah R.K., 1975, Laminar flow friction and forced convection heat transfer in ducts of arbitrary geometry, *Int. J. Heat and Mass Transfer*,18, 849-862.

S.K. Thomas and V.C. Damle, 2005, Fluid flow in axial reentrant grooves with application to heat pipes, *J. Thermophys. Heat Transfer*, 19,395–405.

Suh J. S. and Park Y. S., 2003, Analysis of thermal performance in a micro flat heat pipe with axially trapezoidal groove, *Tamkang Journal of Science and Engineering*, 6, 4, 201–206.

Suman B. and Hoda N., 2005, Effect of variations in thermos-physical properties and design parameters on the performance of a v-shaped micro grooved heat pipe. *International Journal of Heat and Mass Transfer*, 48, 2090-2101.

Vlassov V. V., Sousa F. L. and Takahashi W. K., 2006, Comprehensive optimization of a heat pipe radiator assembly filled with ammonia or acetone, *Int. J. Heat and Mass Transfer*, 49, 4584–4595.

Zohuri B., 2016, *Heat Pipe Design and Technology, Modern Applications for Practical Thermal Management* (2nd Ed.), Spinger, Switzerland.

Cem ÖMÜR graduated from Mechanical Engineering Department of Middle East Technical University in 2007. After working at Ford Motor Company between July 2007 and August 2008 as an Engine Test Engineer, he started working in Turkish Aerospace Industry, Inc. He received his Masters degree in the year 2010 from the Mechanical Engineering (M.E.) Department of Middle East Technical University. He has expertise in the fields of thermal vacuum testing, instrumentation of sensors and spacecraft thermal control and design. He is currently working at TAI as a thermal test engineer and performing his Ph.D. studies at the Mechanical Engineering Department of Gazi University, Ankara, Turkey.

Ahmet Bilge UYGUR graduated from Chemical Engineering Department of Middle East Technical University (Ankara, Turkey) in the year 2000. He received his M. Sc. and Ph. D. degrees from the same department in the years 2002 and 2007, respectively. His principle research interests are Computational Fluid Dynamics, Spacecraft Thermal Control and Design, Thermal Mathematical Model Development, Spacecraft Assembly, Integration and Environmental Testing. He is currently the Chief Engineer of Space Systems Assembly Integration and Test Management in Turkish Aerospace Industries, Inc.

Ilhami HORUZ graduated from Mechanical Engineering Department of Uludag University in the year 1988. Then, he received his M. Sc. degree from the same university and his PhD degree from the University of Strathclyde, U. K. in the years 1990 and 1994, respectively. His principle research interests are heating, refrigeration, air conditioning, renewable energy, energy utilization and fuel cells. He is currently working for the Mechanical Engineering Department of Gazi University as a lecturer.